RSC Advances

ROYAL SOCIETY OF CHEMISTRY

www.rsc.org/advances

Inertia-activated cell sorting of immune-specifically labeled cells in a microfluidic device

Joong Ho Shin, Myung Gwon Lee, Sungyoung Choi and Je-Kyun Park*

This paper demonstrates an inertia-activated cell sorting method to separate cells based on their surface protein expression by using inertial microfluidics.

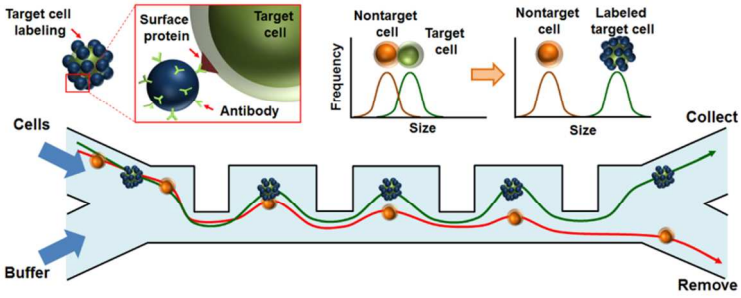

Journal Name

RSCPublishing

ARTICLE

Inertia-activated cell sorting of immune-specifically labeled cells in a microfluidic device

Cite this: DOI: 10.1039/x0xx00000x

Joong Ho Shin,[a] Myung Gwon Lee,[b] Sungyoung Choi[c] and Je-Kyun Park[a]*

Received ooth January 2012,
Accepted ooth January 2012

DOI: 10.1039/x0xx00000x

www.rsc.org/

This paper demonstrates an inertia-activated cell sorting method to separate cells based on their surface protein expression by using inertial microfluidics. Target cells are immune-specifically reacted with antibody-coated microbeads and then separated from nontarget cells. As a proof of concept, separation of MCF-7 breast cancer cells from U937 lymphoma cells was achieved with 97.6% target cell recovery rate, 95% nontarget cell rejection ratio, 73.8% purity, and enrichment ratio of 93 at a total flow rate of 8.75 mL/h without using any external forces.

Separation of specific kind of cells from other cells has been an important part of biological and biomedical research. Conventional cell separation methods that have been widely used are fluorescence-activated cell sorting (FACS) and magnetic-activated cell sorting (MACS).[1] Conventional FACS sorts fluorescently labeled cells and MACS discriminates immunomagnetically labeled cells by using external magnetic field. Although both are extensively used and show wide applications, FACS is expensive, not appropriate for sorting extremely rare cells due to its high reagent consumption, and requires a trained technician for operation and maintenance; while MACS requires several washing steps which make it a time-consuming process and lead to cell loss.

To overcome such limitations of the conventional methods, many lab-on-a-chip platforms are developed by adopting the principle of FACS and MACS. Although miniaturized FACS devices demonstrated successful separation of *Escherichia coli*[2,3] and HeLa cells[4], their complex setup and operation for active sorting require complicated fabrication process and external equipment involving laser excitation and signal detection. Separations of immunomagnetically labeled targets utilizing magnetic field have also been demonstrated on chip for various applications, including continuous separation of magnetically labeled multi target cells,[5] separation of pathogen for blood cleansing,[6] and capture and culture of circulating tumor cells.[7] However, the separation efficiency depends on the duration at which the labeled cells are influenced by magnetic field, which inherently limits the throughput of the active sorting systems.

Recent advances in inertial microfluidics have allowed continuous, high-throughput separation of particles and cells with different sizes by utilizing drag force and inertial lift force, without using any external forces.[8–13] However, inertial microfluidics has an inherent limitation, in which it is difficult to separate cells of the same size and researchers resort to either sacrificing purity for high recovery rate or sacrificing recovery for high purity.[11,14] Thus in this study we exploit immune-specifically labeled target cells with microbeads to enhance their size and differentiate them from nontarget cells, and then demonstrate continuous separation in an inertial microfluidic device with both high purity and recovery rate. Immune-specific size enhancement of target cells causes an increase in inertial lift force, which consequently results in separation from nonlabeled cells; therefore we term this process inertia-activated cell sorting (IACS). As a proof of concept study, MCF-7 breast cancer cells were separated from U937 lymphoma cells to demonstrate that similar sized cells can be effectively separated in an inertial microfluidic device by bead-labeling. The device used in this study is a contraction–expansion array (CEA) microchannel, which has been demonstrated for size-based separations in biomedical fields.[12,15–18] This is, to the best of our knowledge, the first to report the separation of immune-specifically labeled cells using inertial microfluidics.

The CEA microchannel was fabricated by conventional soft lithography technique. The PDMS replica was irreversibly bonded with glass slide by oxygen plasma treatment. The device consists of four arrays, each of which has 150 μm long, 50 μm wide contraction region and 700 μm long, 350 μm wide expansion region, whose channel height is 55 μm. The dimensions and array numbers were chosen by taking previous works as reference[12,15] for optimal U937 and bead-labeled MCF-7 cell separation.

Beads were coated with antibodies that bind to epithelial cell adhesion molecule (EpCAM) first so that they can bind to the proteins expressed on the cell's surface. 5 μm diameter streptavidin coated beads (Bangslab, Fishers, IN) were conjugated with monoclonal anti-human EpCAM/TROP1 biotinylated antibody (R&D Systems, Minneapolis, MN). Beads and antibodies were rotated at 10 rpm on a rotator (PTR-60, Grant-bio, Shepreth, U.K.) for 1 h while being suspended in phosphate buffered saline containing (PBS) 1% bovine serum albumin (BSA) for streptavidin–biotin interaction. Beads were washed three times to remove any unbound antibody, and rotated again at 10 rpm with MCF-7 cells in PBS containing 1% BSA, at 5.73×10^7 beads/mL bead concentration at room temperature for antibody–antigen binding. For characterization of bead-labeled cell's trajectories, MCF-7 cells were incubated with the beads for 1 h and for separation experiment that was performed with U937 cells, MCF-7 cells were incubated with the beads for 2 h. Microscopic images of the bead-labeled cells were taken while the view was focused at the top of the cell

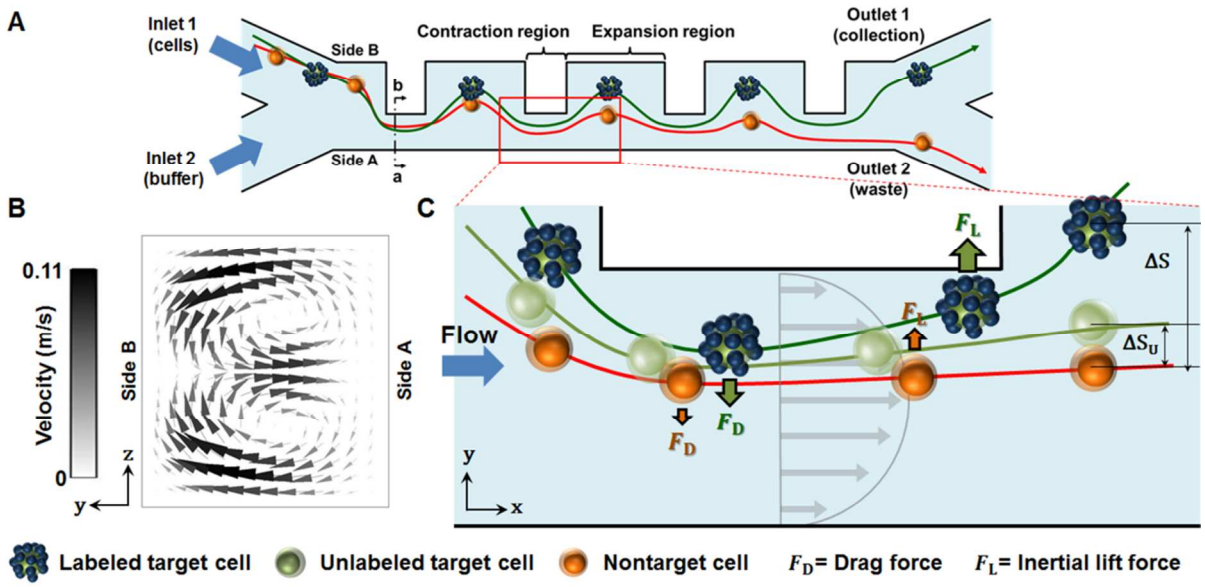

Fig. 1 (A) Schematic of CEA microchannel for size-based separation (Top view). (B) Cross-sectional view (section a–b) of simulated *vw* components of secondary flow at the entrance of the contraction region. (C) Schematic of drag force and inertial lift force on cells passing through the contraction region. The distance between labeled target cell and nontarget cell (ΔS) is greater than the distance between unlabeled target cell and nontarget cell ($ΔS_U$) at the last expansion region.

(away from the glass slide along the *z*-axis) so that the upper part of the cell's surface can be imaged. The coverage of cell–bead labeling is defined as a ratio of surface area occupied with beads to the total cross sectional area of cell–bead complex.[19]

U937, MCF-7, and bead-labeled MCF-7 cells were injected into the device at a concentration of 1.25×10^6, 5×10^5, and 10^4 cells/mL, respectively, for lateral position characterization. 2×10^4 bead-labeled MCF-7 cells were spiked into 2 mL of 1.25×10^6 cells/mL U937 suspension to observe the separation from the mixed solution. Total flow rates tested were 2.19, 4.37, 6.56, and 8.75 mL/h, which are equivalent to Reynolds number (Re) of 3, 6, 9, and 12 when converted with respect to the expansion region dimension.

The CEA microchannel is consisted of series of regions whose width alternately contracts and expands (Fig. 1A). The device utilizes two forces to separate particles based on their size: Drag force induced by secondary flow and inertial lift force. As fluid enters the narrow part of the channel (contraction region) from wider part of the channel (expansion region), fluid molecules from side B accelerate and flow towards side A to enter the contraction region. The direction of the fluid is perpendicular to the direction of the main flow and results in a secondary flow. The secondary flow results in two counter-rotating vortices at the entrance of the contraction region, whose direction at the center of the channel is perpendicular to the main flow direction (Fig. 1B), and causes drag force (F_D) on particles assuming Stokes drag:[16,20]

$$F_D = 3\pi\mu U_{vw} a_p \quad (1)$$

where μ, U_{vw}, and a_p are the viscosity of the fluids, transverse velocity of secondary flow, and particle diameter, respectively. Because focusing buffer is injected from inlet 2 at a flow rate which is nine times greater than that from inlet 1, particles' streamlines are initially focused near the wall of side B before they enter the first contraction region, and the secondary flow causes cells to migrate to side A. The magnitude of the transverse velocity component (*vw)* that directs toward side A and the maximum curl, which represents the rotation of the vortex, increase as the total flow rate increases (see ESI†, Fig. S1A). This indicates that particles passing through the entrance of the contraction region would deflect further to side A by the secondary flow at a higher flow rate due to increased magnitude of drag force.

As particles flow through the contraction region, they are also exposed to shear-induced inertial lift force that arises from the parabolic velocity profile. The inertial lift force causes particles to migrate back toward side B of the channel. The inertial lift force (F_L) is defined as below[20,21]

$$F_L = \frac{\rho U_m^2 a_p^4 C_L}{D_h^2} \quad (2)$$

where ρ, U_m, C_L, and D_h are the density of the fluid, *x*-axial maximum flow velocity, the lift coefficient, and hydraulic diameter, respectively. The inertial lift force has much greater effect on relatively larger particles than it does on smaller particles due to its a_p^4 term. This causes relatively larger particles to migrate back to side B of the channel faster than the smaller particles do (Fig. 1C). As they enter and flow through the next contraction region, drag force causes smaller particles to move further to side A while inertial lift force cause particles to migrate back to side B, resulting in spatial distance between particles' streamlines. Passing through more arrays separates particles further away from each other and results in greater separation resolution. At Re = 12, in a 700 μm wide section of the device (after four arrays of contraction channel), 1 μm difference in a particle's diameter would result in 13.3 μm difference in lateral positions theoretically (see ESI†, Fig. S1B). Particles' lateral positions span across the channel width with smaller particles near side A and larger particles near side B.

On the basis of this characterization of the CEA device, we labeled the target cells with antibody-coated microbeads to increase their overall size. Although the average sizes of U937 and MCF-7 cells are different, U937 cells (average diameter = 13.29 ± 1.40 μm) and MCF-7 cells (17.65 ± 3.11 μm), there is an overlap in the size distribution (Fig. 2A), which is the population that cannot be separated by conventional inertial

size-based separation. However, labelling MCF-7 cells with 5 μm beads selectively amplifies the size of the cells (28.13 ± 3.17 μm) and eliminates the size overlap, allowing them to be separated from U937 cells. Bead labeling increases the effect of inertial lift force that arises from increased diameter, which would theoretically be greater compared to nonlabeled MCF-7 cells by a factor of 6.45 (according to the a_p^4 term in the inertial lift force equation). The extents to which MCF-7 cells are covered by beads vary even from the same batch as shown in ESI† Fig. S2. The coverage obtained with 5 μm bead labeling was calculated to be 90.97% (n = 18), which suggests that the variation in the increased amount of inertial lift force by the size enhancement is inconsiderable due to uniformly increased size.

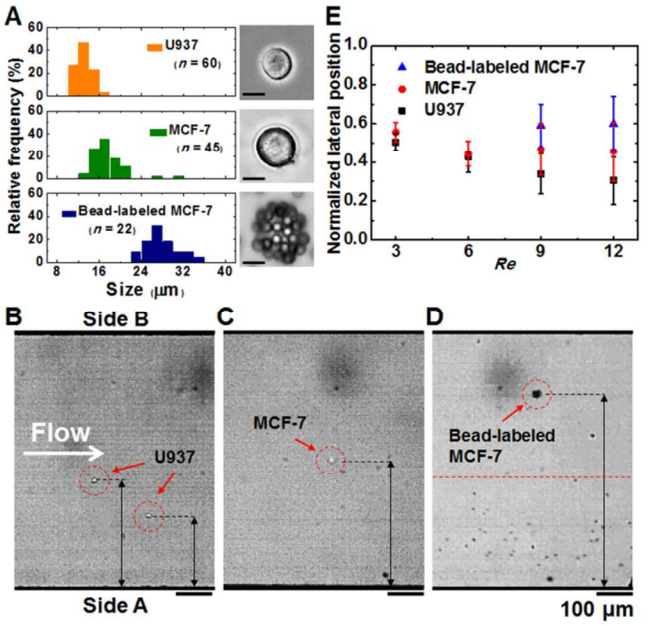

Fig. 2 A) Size distribution of U937, MCF-7 cells, and MCF-7 cells labeled with 5 μm beads with pictures on the right. Scale bars = 10 μm. Image of B) U937, C) MCF-7 cells, and D) bead-labeled MCF-7 cells captured at a wide section of CEA microchannel after passing through four arrays at Re = 12. Unbound 5 μm beads' lateral positions are between side A and the red dotted line. E) The lateral positions of U937, MCF-7 cells versus Re, and the lateral positions of bead-labeled MCF-7 cells at Re values of 9 and 12.

To characterize the inertial migration of cells in a CEA microchannel, different kinds of cells were injected separately into the device and their lateral positions were imaged at the expansion region by using a high-speed camera (HotShot 512 sc; NAC, Simi Valley, CA). White spheres are identified as U937 and MCF-7 cells (Fig. 2B, C). For bead-labeled MCF-7 cells, small black spots are identified as unlabeled 5 μm beads and round black spheres are identified as bead-labeled MCF-7 cells (Fig. 2D). The images were analyzed with ImageJ software to measure the distance from the channel wall of side A, and the average lateral positions were normalized as values between 0 to 1, spanning from side A to side B.

Fig. 2E shows that U937's average lateral position approaches side A with increasing Re due to dominant effect of secondary flow-induced drag force. Unlabeled MCF-7 cell's average lateral position remains approximately at the center of the channel width for all Re, which indicates that the effect of drag force and inertial lift force are balanced. Although at Re = 9 and 12, U937 and unlabeled MCF-7 cells have distinct average lateral positions, there are overlaps in the lateral positions as shown by the error bars. The overlap in lateral position of the cells arises from the overlap in U937 and MCF-7 cell's size distribution and it shows the limitation of size-based separation of similar sized cells. Unlike the unlabeled MCF-7 cells, MCF-7 cells labeled with 5 μm diameter beads result in average lateral positions which are further away from that of U937's lateral positions (closer to side B) at Re = 9 and 12. This indicates that immune-specific labeling can reduce the lateral position overlap between U937 and MCF-7 cells, which would result in increased separation efficiency. As shown in Fig. 2D, unbound 5 μm beads were observed between side A and red dotted line, which means that they will not be collected along with the target cells.

To demonstrate that cell separation can be performed from mixed sample, bead-labeled MCF-7 cells were spiked into a suspension of U937 cells and then their lateral positions were observed at Re = 12. As shown in Fig. 3A, U937 cells were observed closer to side A, while bead-labeled MCF-7 cells were observed near side B. By bifurcating the channel width in half, labeled target cells can be collected from outlet 1 and nontarget cells can be removed from outlet 2 along with unbound 5 μm beads.

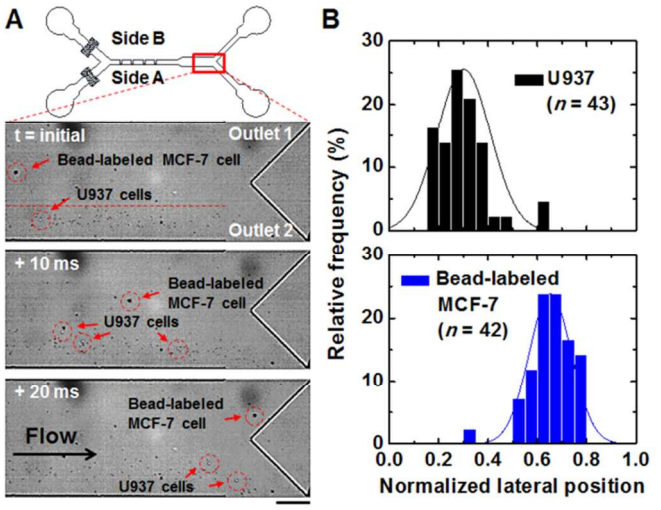

Fig. 3 A) Image of U397 cells and bead-labeled MCF-7 cells at the wide section of the CEA microchannel at Re = 12. Unbound 5 μm beads' lateral positions are between side A and the red dotted line. Scale bar = 200 μm. B) The distribution of lateral positions of U937 cells and bead-labeled MCF-7 cells.

Separation efficiency was evaluated by calculating the recovery rate, the rejection ratio, purity, and enrichment ratio. Each represents how well the device can collect the target cells without losing them, how well it can remove nontarget cells, how much the collected sample is free of contaminants, and how much the fraction of the target cell is increased after the separation. The values were calculated by splitting the channel width in half and counting the number of cells with respect to the center (0.5 times the width). The cells observed between 0 and 0.5 of the normalized channel width are considered to be wasted through outlet 2 and between 0.5 and 1 are considered

to be collected from outlet 1. Recovery rate is a ratio of MCF-7 cells collected from the upper outlet to total number of MCF-7 cells that flowed out through both upper and lower outlet, defined as:

$$\frac{MCF\text{-}7_{\text{outlet 1}}}{MCF\text{-}7_{\text{outlet 1}} + MCF\text{-}7_{\text{outlet 2}}} \quad (3)$$

The U937 rejection ratio is a ratio of U937 cells that are removed through outlet 2 to the total number of U937 cells, defined as the following equation:

$$\frac{U937_{\text{outlet 2}}}{U937_{\text{outlet 1}} + U937_{\text{outlet 2}}} \quad (4)$$

The purity is a ratio of the collected MCF-7 cells to the total number of cells collected from the outlet 1, defined as:

$$\frac{MCF\text{-}7_{\text{outlet 1}}}{MCF\text{-}7_{\text{outlet 1}} + U937_{\text{outlet 1}}} \quad (5)$$

The enrichment ratio is a ratio of the purity of the collected sample divided by the purity of the injected sample, defined as:

$$\frac{(MCF\text{-}7/U937 + MCF\text{-}7)_{\text{outlet 1}}}{(MCF\text{-}7/U937 + MCF\text{-}7)_{\text{inlet 1}}} \quad (6)$$

The recovery rate is calculated to be 97.6%, rejection ratio is 95%, purity is 73.8%, and enrichment ratio is 93 (spiked sample purity = 0.79%) at a total flow rate of 8.75 mL/h. As shown in the histograms in Fig. 3B, it is clear that the lateral positions of U937 cells and bead-labeled MCF-7 cells are distinct from each other. The altered lateral positions of MCF-7 cells caused by bead labeling results in effective separation from U937 cells due to increased effect of inertial lift force. These results show that IACS is capable of sorting cells that express different surface proteins despite having the same size.

Although EpCAM expressing cell was separated as an example in this paper, the application is not limited to EpCAM positive cells. The surface of the beads can be functionalized with other antibodies that are specific to target antigens of interest and be used to separate cells that express other surface protein other than EpCAM to fit the researcher's needs.

As the labeling efficiency depends on the number of beads and incubation time, further protocol may need to be optimized for consistent labeling that requires minimum number of beads. The current cost for cell labeling in this study is approximately $250 per test considering the retail price of antibodies and microbeads, however, the price can be reduced through optimization of the labeling protocol. Furthermore, the total surface area of the beads functionalized in this study is 0.0022 m^2 per test. Devices like CTC chip[22] and geometrically activated surface interaction (GASI) chip[23] captures EpCAM expressing CTCs by utilizing collision of CTCs to antibody coated microposts or microfluidic channel wall. The total surface area of 78,000 microposts that need to be covered in CTC chip is 0.0024 m^2 per chip and the conservative estimate of the surface area of the eight microfluidic channels of GASI chip is 0.0017 m^2 without considering the extra surface extruded by microgrooves. Thus, the price of antibodies used to coat the microbeads is not expected to greatly surpass the cost to produce the mentioned antibody coated microfluidic devices.

For clinical and research purposes, red blood cells (RBCs) should be removed from blood sample before labeling target cells for effective labeling. Alternatively, a possible solution for reduced handling of blood samples is an integration of RBC removing part[17] and cell–bead labeling part[24] with the proposed CTC separation device. An integrated lab-on-a-chip device with such configuration would allow on-chip RBC removal and target cell labeling with single injection step of whole blood sample.

Although the study focused on observing the effect of size-enhancement on inertial effect, using magnetic particles and magnetic field is also expected to further increase the separation efficiency. For example, magnetic nanoparticles can be used as an additional labeling to bind with surface proteins that are not labeled by microbeads after size-enhancement; or cells can be labeled by using micro-sized magnetic particles for size-enhancement effect and additional effect of magnetic force. Furthermore, considering the fact that the variation of EpCAM expression level in different EpCAM positive cell lines range from as low as 1,700 antigens per cell (MDA-MB-231 breast cancer cells) to as high as 222,000 per cell (MCF-7 cells),[24] immune-specifically enhancing the size of cells of low expression level may not be as effective as labeling cells of high expression level. Separation of such cells may benefit from magnetic particle labeling.

For further analysis that require staining of the collected cells, the beads will be removed by using commercially available buffers such as stripping buffers, which are widely used for Western blot for the purpose of removing antibody from antigen. As reported in a previous study,[25] molecular profiles of cells can be analyzed by flow cytometry after removing surface bound antibodies from the cells' surface with stripping buffer, which shows the possibility of further analyzing the separated samples that are collected from outlet 1.

In summary, we have described a method to separate cells based on their difference in surface protein expression by immune-specific labeling and using inertial microfluidics. U937 cells and MCF-7 cells were chosen as an example to represent two cell populations whose average sizes are different but have overlapping sizes. The result suggests that immune-specific labeling for size enhancement can be applied to other inertial microfluidic devices to overcome their current limitation and help separate target cells with higher efficiency. One of the advantages of the inertial microfluidics is that it requires no external forces and optical instruments. Thus the system can be cheaper, simpler and easier to fabricate compared to other microfluidic separation systems, and it is expected to help facilitate and contribute in many areas of studies, including biological and biomedical researches that require cell separation.

Acknowledgements

This research was supported by a Converging Research Center Program (Grant 2011K000864) and a National Leading Research Laboratory Program (Grant NRF-2013R1A2A1A05006378) through the National Research Foundation of Korea funded by the Ministry of Science, ICT and Future Planning. The authors also acknowledge a National Academy of Agricultural Science Program (Grant PJ009842) supported by Rural Development Administration, Korea.

Notes and references

[a] Department of Bio and Brain Engineering, Korea Advanced Institute of Science and Technology (KAIST), 291 Daehak-ro, Yuseong-gu, Daejeon 305-701, Republic of Korea

[b] Intellectual Discovery Co,. Ltd., 511 Samseong-ro, Gangnam-gu, Seoul 135-745, Republic of Korea

[c] Department of Biomedical Engineering, Kyung Hee University, 1732 Deogyeong-daero, Gilheung-gu, Yongin-si, Gyeonggi-do 446-701, Republic of Korea

†Electronic Supplementary Information (ESI) available: Figs. S1 and S2. See DOI: 10.1039/b000000x/

1 A. Radbruch and D. Recktenwald, *Curr. Opin. Immunol.*, 1995, **7**, 270–273.

2 A. Y. Fu, C. Spence, A. Scherer, F. H. Arnold and S. R. Quake, *Nat. Biotechnol.*, 1999, **17**, 1109–1111.

3 J. -C. Baret, O. J. Miller, V. Taly, M. Ryckelynck, A. El-Harrak, L. Frenz, C. Rick, M. L. Samuels, J. B. Hutchison, J. J. Agresti, D. R. Link, D. A. Weitz and A. D. Griffiths, *Lab Chip*, 2009, **9**, 1850–1858.

4 M. M. Wang, E. Tu, D. E. Raymond, J. M. Yang, H. Zhang, N. Hagen, B. Dees, E. M. Mercer, A. H. Forster, I. Kariv, P. J. Marchand and W. F. Butler, *Nat. Biotechnol.*, 2005, **23**, 83–87.

5 J. D. Adams, U. Kim and H. T. Soh, *Proc. Natl. Acad. Sci. U.S.A.*, 2008, **105**, 18165–18170.

6 C. W. Yung, J. Fiering, A. J. Mueller and D. E. Ingber, *Lab Chip*, 2009, **9**, 1171–1177.

7 J. H. Kang, S. Krause, H. Tobin, A. Mammoto, M. Kanapathipillai and D. E. Ingber, *Lab Chip*, 2012, **12**, 2175–2181.

8 D. Di Carlo, D. Irimia, R. G. Tompkins and M. Toner, *Proc. Natl. Acad. Sci. U.S.A.*, 2007, **104**, 18892–18897.

9 S. S. Kuntaegowdanahalli, A. A. S. Bhagat, G. Kumar and I. Papautsky, *Lab Chip*, 2009, **9**, 2973–2980.

10 A. J. Mach, J. H. Kim, A. Arshi, S. C. Hur and D. Di Carlo, *Lab Chip*, 2011, **11**, 2827–2834.

11 E. Sollier, D. E. Go, J. Che, D. R. Gossett, S. O'Byrne, W. M. Weaver, N. Kummer, M. Rettig, J. Goldman, N. Nickols, S. McCloskey, R. P. Kulkarni and D. Di Carlo, *Lab Chip*, 2014, 63–77.

12 M. G. Lee, J. H. Shin, S. Choi and J. -K. Park, *Sens. Actuators B Chem.*, 2014, **190**, 311–317.

13 K. -A. Hyun, K. Kwon, H. Han, S. -I. Kim and H. -I. Jung, *Biosens. Bioelectron.*, 2013, 206–212.

14 M. E. Warkiani, G. Guan, K. B. Luan, W. C. Lee, A. A. S. Bhagat, P. Kant Chaudhuri, P. K. Chaudhuri, D. S. -W. Tan, W. -T. Lim, S. C. Lee, P. C. Chen, C. T. Lim and J. Han, *Lab Chip*, 2014, **14**, 128–137.

15 M. G. Lee, S. Choi, H. -J. Kim, H. K. Lim, J. -H. Kim, N. Huh and J. -K. Park, *Appl. Phys. Lett.*, 2011, **98**, 253702.

16 M. G. Lee, S. Choi and J. -K. Park, *J. Chromatogr. A*, 2011, **1218**, 4138–4143.

17 M. G. Lee, J. H. Shin, C. Y. Bae, S. Choi and J. -K. Park, *Anal. Chem.*, 2013, **85**, 6213–6218.

18 J. Lee, M. G. Lee, C. Jung, Y. -H. Park, C. Song, M. C. Choi, H. G. Park and J. -K. Park, *BioChip J.*, 2013, **7**, 210–217.

19 M. S. Kim, T. S. Sim, Y. J. Kim, S. S. Kim, H. Jeong, J. -M. Park, H. -S. Moon, S. I. Kim, O. Gurel, S. S. Lee, J. G. Lee and J. C. Park, *Lab Chip*, 2012, **12**, 2874–2880.

20 D. Di Carlo, *Lab Chip*, 2009, **9**, 3038–3046.

21 E. S. Asmolov, *J. Fluid Mech.*, 1999, **381**, 63–87.

22 S. Nagrath, L. V. Sequist, S. Maheswaran, D. W. Bell, D. Irimia, L. Ulkus, M. R. Smith, E. L. Kwak, S. Digumarthy, A. Muzikansky, P. Ryan, U. J. Balis, R. G. Tompkins, D. A. Haber and M. Toner, *Nature*, 2007, **450**, 1235–1239.

23 K. -A. Hyun, T. Y. Lee and H. -I. Jung, *Anal. Chem.*, 2013, **85**, 4439–4445.

24 M. X. Lin, K. -A. Hyun, H. -S. Moon, T. S. Sim, J. -G. Lee, J. C. Park, S. S. Lee and H. -I. Jung, *Biosens. Bioelectron.*, 2013, **40**, 63–67.

25 B. Gao, T. Curtis, F. Blumenstock, F. Minnear and T. Saba, *J. Cell Sci.*, 2000, **113**, 247–257.